Effects of molecule anchoring and dispersion on nanoscopic friction under electrochemical control

A. S. de Wijn,[1, *] A. Fasolino,[2] A. E. Filippov,[3] and M. Urbakh[4]

[1]*Department of Physics, Stockholm University, 106 91 Stockholm, Sweden*
[2]*Radboud University, Institute for Molecules and Materials,*
Heyendaalseweg 135, 6525AJ Nijmegen, the Netherlands
[3]*Donetsk Institute for Physics and Engineering of NASU, 83144, Donetsk, Ukraine*
[4]*School of Chemistry, Tel Aviv University, 69978 Tel Aviv, Israel*

The application of electric fields is a promising strategy for *in situ* control of friction. While there have recently been many experimental studies on friction under the influence of electric fields, theoretical understanding is very limited. Recently, we introduced a simple theoretical model for friction under electrochemical conditions focusing on the interaction of a force microscope tip with adsorbed molecules whose orientation depends on the applied electric field. Here we focus on the effects of molecule anchoring on friction. We show that the anchoring affects the intensity and width of the peak in the friction that occurs near a reorientation transition of adsorbed molecules, and explain this by comparing the strengths of molecule-molecule and molecule-tip interactions. We derive a dispersion relation for phonons in the layer of adsorbed molecules, and demonstrate that it can be used to understand important features of the frictional response.

PACS numbers:

I. INTRODUCTION

One of the main challenges in tribology is finding a way for in situ control of friction without having to change the lubricant. A promising strategy for such control is via the application of electric fields in experiments performed under electrochemical conditions where the properties of the electrode-electrolyte interface depend on the applied potential bias. Despite numerous experimental results [1–16], however, understanding of the molecular origin of the observed friction response to variation of applied potential remains challenging. The interface formed by a solid surface with adsorbates and the electrode in a polar liquid is extremely complex, due to the complicated molecule anchoring and presence of several different mechanisms of dissipation. For these reasons, simple qualitative models designed to understand the basic mechanisms are desirable before attempting detailed molecular dynamics studies.

Much progress in understanding of friction on the nanoscale has been based on two simple one-dimensional models: the Prandtl-Tomlinson (PT) and Frenkel-Kontorova (FK) models [17]. These models, however, cannot describe shear induced dynamics at solid-liquid interfaces, and in particular the effects due to reorientation of adsorbed molecules on friction. For this purpose, we have recently proposed a similarly simple model suitable for the description of friction in electrochemical conditions [18]. We have represented the adsorbed molecules as rigid dipoles and considered only their low-energy rotations as a whole as a possible source of energy dissipation. We found that the dependence of the friction force on the electric field is determined by the interplay of two channel of energy dissipation: (i) the rotation of dipoles and (ii) slips of the tip over potential barriers. Within this model, the reorientation in an external electric field and the interactions with a scanning tip can justify qualitatively the observed drastic changes of friction with field. Here we enrich the model in two ways by (i) considering two different types of anchoring of the adsorbates and (ii) elucidating the mechanism of frictional dissipation by establishing a quantitative correlations between the calculated changes of friction in a field with the phonon spectrum of the dipoles in different anchoring configurations.

Our aim is to provide a basis for general understanding of overall trends and effects of the new parameters introduced by electrostatic interactions in electrolyte systems, rather than to study a specific system. Nevertheless, we are motivated to investigate friction under electrochemical control by the rapid recent experimental developments in this area. Studies of friction at the macroscopic scale have demonstrated the possibility to control friction in metal/metal and metal/ceramic contacts lubricated with aqueous-based solutions, where the coefficient of friction can be altered over a wide range by application of an external electrical potential [1–4]. At the atomic scale, friction force microscopy (FFM) has been used to study the potential dependence of friction at steps on highly orientated pyrolytic graphite (HOPG) surfaces [5], as well as frictional changes due to reconstruction, oxidation, and adsorption of anions and metallic adatoms and reorientation of adsorbed molecules at metal electrodes [5–12]. Recently results of the first SFA (surface force apparatus) measurements under electrochemical potential control between a metal and a ceramic surface across a liquid medium (water) have been reported [13]. These studies show clear and reproducible variation of friction coeffi-

———————
[*]Electronic address: astrid@dewijn.eu

cient with potential and electrochemical conditions. One of the most extensively studied adsorption processes in electrochemistry is the pyridine adsorption on gold surfaces, where a change in the orientation of the aromatic ring in the pyridine molecule as a function of applied potential have been observed [14, 15]. At negatively charged surfaces (below the point of zero charge), the ring lays flat on the gold surface, while at more positive potentials, it flips and stands up with the nitrogen atom on the surface, thereby allowing increased surface concentration. The first FFM measurements of pyridine adsorption on gold electrodes under electrochemical potential control demonstrated a considerable increase of friction at the potential where the transition from horizontal to vertical orientation occurs [16]. The adsorption and reorientation of pyridine are both reversible, making the pyridine-gold system a promising model for the implementation of active control of friction.

The different systems of interest for experiments constitute the motivation to extend the model previously proposed [18] with the purpose to understand the influence of field-induced dynamics of adsorbed molecules like water and anchored molecules like pyridine where also steric hindrance becomes important. In Sec. II we introduce the model. In Sec. III, we show numerical results the friction as a function of the applied potential. We compare different geometries, and explain how the anchoring affects the dynamics and through it the friction. In Sec. IV, we compute the dispersion relation for the model, and use it to explain an additional feature in the friction. Finally, in Sec. V we summarise our results.

II. MODEL

Our model is illustrated in Fig. 1. To mimic a typical FFM experiment, in the same style as the Prandtl-Tomlinson model, we consider a tip with mass M and center-of-mass (com) coordinate X, coupled by a spring of spring constant K to a support that moves at constant velocity v_s. The polar molecules adsorbed at the electrode are represented simply by rigid dipoles that interact with each other, the tip, and an external field.

In our previous work [18], we considered dipoles that were able to rotate only around their center of mass. This simplified description captures the essence of the potential-induced reorientation of molecules such as water on metal electrodes [19–22]. This choice of anchoring of the molecules however does not mimic the reorientation of the majority of adsorbed molecules, such as pyridine, which are anchored to the surface by one of its outer atoms.

Here we extend the model to study the effects of anchoring and molecule anchoring on the change in friction near the reorientation transition. In this work we allow for two different types of anchoring: the dipoles are anchored to the surface either by their centers of mass, or by the negatively-charged end. If the dipoles are anchored
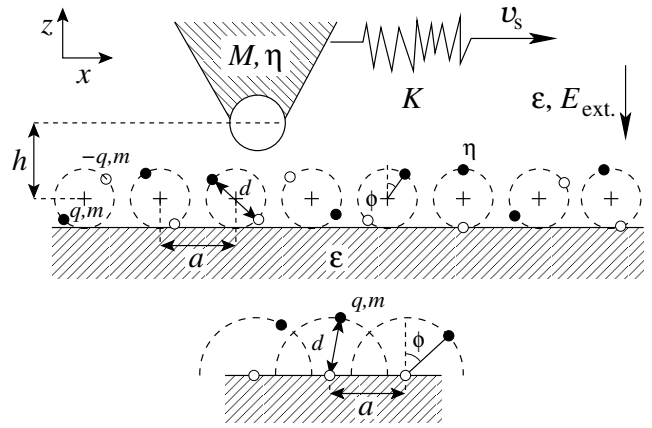
FIG. 1: A tip is dragged over a surface covered by a monolayer of polar molecules, in the presence of an external electric field E_{ext}. The molecules are either anchored by their center of mass (top), or by the negatively-charged end (bottom). In figures we use the abbreviations "com a." for center-of-mass anchoring, and "end a." for end anchoring.

at one end, we also introduce a repulsive interaction between the surface and other end of the dipole. This ensures that the dipoles cannot behave unphysically and point into the surface. In the absence of external interactions, the dipoles lie horizontally, head-to-tail on the surface at fixed positions.

The external electric field E_{ext} is pointed perpendicular to the surface in the z direction, and is constant. We consider only short range chemical interactions between the dipoles and the tip. The tip is dragged along the surface at a height h from the centers of the dipoles in the upright position. The time average of the lateral force F_{lat}, i.e. the tension in the spring, gives the friction force.

Each dipole consists of two charges $+q$ and $-q$ and masses m separated by a fixed distance d. The N dipoles are arranged in a chain with spacing a with periodic boundary conditions and nearest-neighbour interaction. They can rotate only around their center of mass or around one end.

In order to be able to elucidate the effects of the anchoring by comparing to the old results of Ref [18], we use the same parameter values for charge, mass, and distance, regardless of the anchoring, i. e. the same as in Ref [18], those of water on Pt(111). We have $q = 6.44 \times 10^{-20}$C, $m = 6.42 \times 10^{-26}$kg and $d = 0.958$Å which yield the correct dipole moment and moment of inertia of water molecules (6.17×10^{-30}Cm and 2.95×10^{-46}kgm^2). We use $a = 2.77$Å as the lattice spacing of Pt and $h = d$.

The dipoles interact with their nearest neighbors through electrostatic interactions $V_e(r) = q_1 q_2/(4\pi\epsilon_0 \epsilon r)$, where r is the distance between the two charges q_1 and q_2, and ϵ is the relative electric permittivity of the aqueous solution at the surface. We use $\epsilon = 5$, as estimated by measurements of the double layer capacitance at metal-electrolyte interfaces [23, 24]. We neglect interactions between dipoles beyond nearest neighbors under the as-

sumptions that such interactions are screened due to the ions located in the diffuse part of the double layer.

The tip is modeled as a single particle with no charge. The support velocity is $v_s = 10 \text{m/s}$, which is sufficiently low for the system to exhibit stick-slip behavior. Unless otherwise stated, there is a short-range chemical interaction between the atoms of the tip and one end of the dipoles. However, we also investigate interaction with both ends of the dipoles. This chemical interaction is modeled by the repulsive potential

$$V_c(r) = V_{c0} \exp(-r^2/\sigma_0^2) , \tag{1}$$

where the energy and length scales, V_{c0} and σ_0, are taken as 0.5eV and $\frac{1}{2}a$ respectively.

The temperature T is controlled by a Langevin thermostat with damping constant $\eta = 1/\text{ps}$ on the tip and dipoles. This corresponds to the typical time scales of interactions between the tip or dipoles and their environment. For simplicity we take these two time scales to be equal. The equations of motion thus take the form

$$\ddot{X} = -\frac{K}{M}(X - v_s t) - \frac{1}{M}\frac{\partial}{\partial X}V^{t-d}$$
$$\quad - \eta\dot{X} + \xi_{tip}(t) , \tag{2}$$
$$\ddot{\phi}_i = -\frac{1}{I}\frac{\partial}{\partial \phi_i}\left[V^{d-d} + V^{t-d} + V^{d-s}\right]$$
$$\quad - \eta\dot{\phi}_i + \xi_i(t) - \frac{dq}{I}E_{ext}\sin\phi_i , \tag{3}$$

where ϕ_i is the angle of the i-th dipole with respect to the z-axis, I is the moment of inertia of a dipole, $\xi_{tip}(t)$ and $\xi_i(t)$ are the random forces of the thermostat, and the potentials V^{t-d}, V^{d-d}, and V^{d-s} describe the tip-dipole, dipole-dipole, and dipole-surface interactions that are given by

$$V^{t-d} = \sum_i V_i^{tip}(X) , \tag{4}$$
$$V^{d-d} = \sum_i V_{dipole}(\phi_i, \phi_{i+1}) , \tag{5}$$
$$V^{d-s} = \sum_i V_{surface}(\phi_i) . \tag{6}$$

Here,

$$V_{dipole}(\phi_i, \phi_j) = qq[V_e(|\vec{r}_{i+} - \vec{r}_{j+}|) + V_e(|\vec{r}_{i-} - \vec{r}_{j-}|)$$
$$\quad - V_e(|\vec{r}_{i+} - \vec{r}_{j-}|) - V_e(|\vec{r}_{i-} - \vec{r}_{j+}|)] , \tag{7}$$

with $\vec{R} = (X, h)$, and $\vec{r}_{i+}$ and $\vec{r}_{i-}$ the positions of the positive and negative charges of the ith dipole.

To elucidate the effect of the molecule anchoring, we first compare the equilibrium polarization of the dipoles as a function of field strength for a constant external field. This is shown in Fig. 2. In the ground state, when all dipoles point in the same direction, without any additional force, the potential energy is the same for both
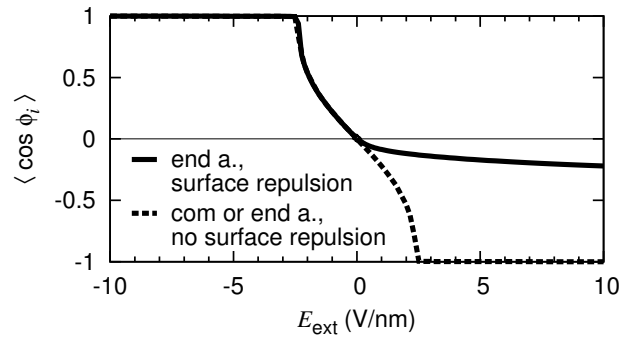
FIG. 2: Polarisation as a function of external field for different anchoring and surface repulsion, at T=2.93 K. Center-of-mass and end anchoring show the same response to the field as long as the dipoles are not pointing into the surface.

types of anchoring. Consequently, the polarization is independent of anchoring. For strong negative fields, the dipoles stand upright. An abrupt reorientation transition occurs at a field strength of -2.4 V/nm. Above this field strength, the dipoles lie approximately flat on the surface. For center-of-mass anchoring, we have previously shown that near this reorientation transition the friction peaks [18].

Due to symmetry, there is another reorientation transition at +2.4 V/nm, above which the dipoles point down into the substrate. For dipoles anchored by one end, this is unphysical. Therefore, for dipoles with end anchoring we introduce a repulsive interaction between the mobile end and the substrate, which changes the polarization for positive fields. If the dipoles are anchored by one end, then, unless otherwise stated, the other end has a repulsive interaction with the substrate of the form

$$V_{surface}(\phi_i) = \begin{cases} 16(\cos\phi)^4 V_0 & \text{if } \phi > \pi/2 \\ 0 & \text{otherwise} \end{cases} . \tag{8}$$

This form was chosen so that there are no additional forces as long as the dipoles are pointing out of the substrate and the transition is preserved exactly. In addition, the fourth power ensures that the forces are continuous differentiable sufficiently many times to preserve the accuracy of the fourth order Runge-Kutta time integration. In all other cases $V_{surface}(\phi_i) = 0$. The effect of the surface repulsion on the polarization is shown in Fig. 2, where one can see that dipoles anchored by one of the ends no longer point into the substrate for positive external fields.

In almost all cases there is only interaction between the tip and one end of the dipole,

$$V_i^{tip}(X) = \sum_j V_c(|\vec{R} - \vec{r}_{i+}|) . \tag{9}$$

If there is interaction with both ends, then there is a second term in the sum of $V_c(|\vec{R} - \vec{r}_{i-}|)$.
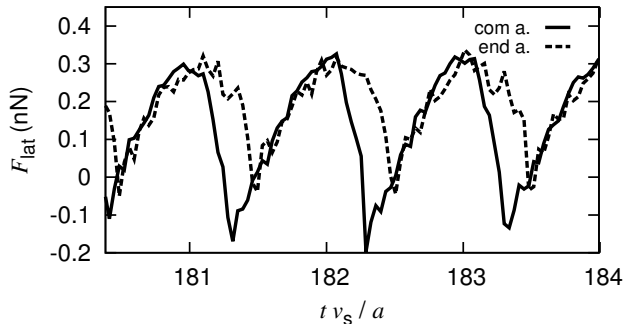
FIG. 3: Lateral force as a function of time for external field strength -5 V/nm for center-of-mass (com) and -9 V/nm for end anchoring.

FIG. 4: Field-dependence of friction, comparison between center-of-mass and end anchoring. The peak in the friction that is related to dipole rotation, is broader, higher, and shifted towards more negative fields. It survives at high temperatures.

As we are interested in the dissipation mechanisms, we must consider the channels through which energy enters and leaves the system. Energy is pumped into the system through the support, with average power $v_s \langle F_{lat} \rangle$ and through thermal noise at an average rate of ηkT per degree of freedom. Energy is removed from the system through the viscous damping of the dipoles and tip. The power dissipated by the i-th dipole can be written as $\dot{\phi}_i \cdot (\eta I \dot{\phi}_i) = 2\eta K_i^d$, where K_i^d is the kinetic energy of the dipole. With a constant external field, the contribution to the average lateral force due to dipole rotations away from equilibrium is thus

$$F_{rot} = \frac{\eta}{v_s} \sum_i (2\langle K_i^d \rangle - kT) . \qquad (10)$$

III. FRICTION RESPONSE

Fig. 3 shows the lateral force as a function of displacement for center-of-mass and end anchoring, at external field strength corresponding to the maximum in the friction, -5 V/nm and -9 V/nm respectively. For both types of anchoring the system displays the typical saw-tooth shape of stick-slip friction, though it is somewhat less pronounced for end anchoring.

We have calculated the friction force as a function of the external field, especially focussing on the peak that results from the reorientation transition. This is shown in Fig. 4 where end anchoring is compared to center-of-mass anchoring [18]. In both cases, there is a peak in the friction near, but not at, the reorientation transition of the dipoles in the field. The dotted line representing $\eta M v_s + F_{rot}$ closely follows the peak and thus shows that for end anchoring the peak in friction is dominated by dipole rotation, as it is also in the case of center-of-mass anchoring [18]. However, the peak is higher, broader and shifted towards more negative fields. There is also a sharp peak at weak fields, which is related to a pathological phonon dispersion at very weak fields, which will be discussed in Sec. IV.
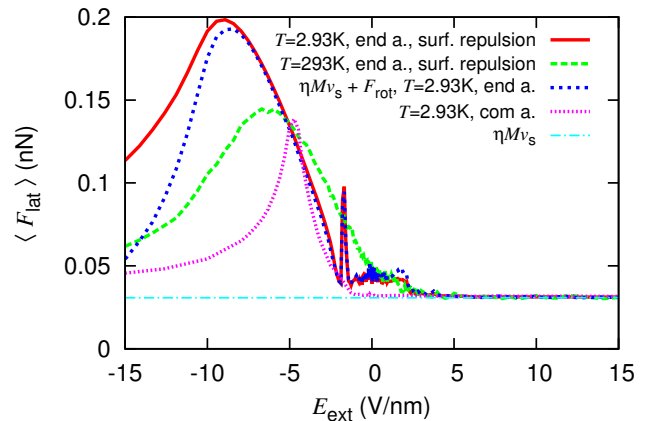
We have not included in the plot the friction for the unphysical systems without the surface repulsion. Our simulations have shown that there is little difference between the friction with and without surface repulsion, because for sufficiently strong negative fields, the dipoles almost always point away from the surface, and are not affected by the surface repulsion. Only at weak fields, where the dipoles spend a significant amount of time pointing into the substrate, there are some small changes. This can also be seen from Fig. 5, which shows the average polarization as a function of the distance to the tip for different anchoring conditions and external potentials. Close to the tip, the dipoles orientation changes. The change in orientation is less for stronger fields, but remains bigger for end anchoring, as can be seen from the dash-dotted line at $E_{ext} = -10$ V/nm. With the surface repulsion, the dipoles can no longer point deeply into the substrate. This only affects their orientation strongly at positive and weakly negative values of the external potential.

The shift of the friction peak towards stronger negative fields of end anchoring with respect to center-of-mass anchoring can be understood as follows. The peak is the result of a dynamic competition between the effects of the external field on the dipoles and the effects of the tip on the dipoles. This is represented schematically in Fig. 6a and b. When the dipoles are anchored in their center of mass, the external field works on both charges, whereas for end anchoring the field affects only one charge. Meanwhile, in both cases, the tip affects just one end. Consequently, the torque on the dipole due to the field is approximately halved for end anchoring, while the dipole-tip interaction strength remains the same. The field strength for which the two interactions are roughly the same thus shifts by approximately a factor of two towards stronger fields. Hence, the peak in the friction that results from this competition shifts as

(a)

(b)

E_{ext}=5 V/nm
E_{ext}=0 V/nm
E_{ext}=-2.5 V/nm
E_{ext}=-5 V/nm
E_{ext}=-10 V/nm

com anchoring

E_{ext}=5 V/nm
E_{ext}=0 V/nm
E_{ext}=-2.5 V/nm
E_{ext}=-5 V/nm
E_{ext}=-10 V/nm
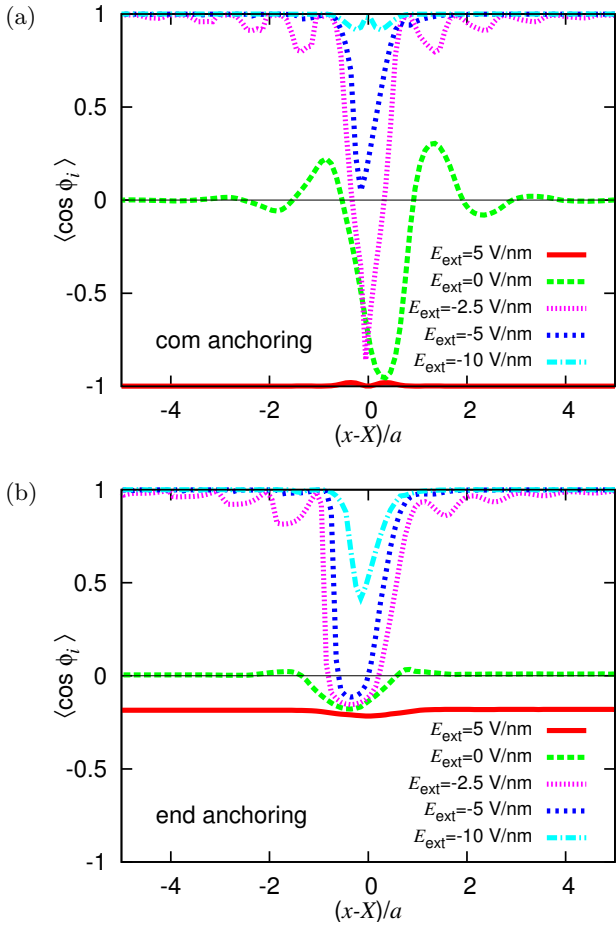
end anchoring

FIG. 5: Comparison of polarization as a function of the distance to the tip for different fields [(a) center-of-mass anchoring, and (b) end anchoring with surface repulsion]. The dipoles reorient near the tip, if the influence of the external field is sufficiently weak.

well, from around -5 V/nm for center-of-mass anchoring to around -9 V/nm for end anchoring. To confirm this picture, we have run simulations with the tip-dipole interaction strength reduced by a factor of two as well, i.e. $V_0 = 250$ meV instead of 500 meV. Results from these simulations are shown in Fig. 7. When the tip-dipole interaction is reduced by a factor of two as well, the peak shifts back to its original position around -5 V/nm.

To further investigate the competition between tip and field, we have also considered the possibility of short-range interaction between the tip and both ends of the dipoles. Results from these simulations, with center-of-mass anchoring, are shown in Fig. 8. The friction for the case of only one chemically interacting end is plotted as well, for comparison. In this case, due to the symmetry of the molecules, two peaks in the friction appear, at positive and negative external potentials of the same magnitude. The absolute value of the potential at which the peak appears is reduced in the case of two interacting ends. When the tip is over a particular dipole, the two torques have opposite sign, and thus the interaction is ef-
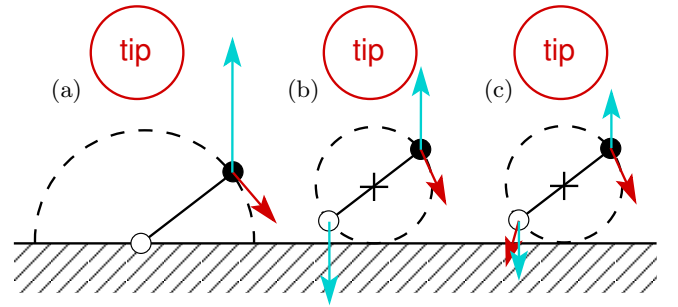
FIG. 6: The forces acting on the two ends of the rigid dipoles in three different cases: (a) end anchoring, (b) center-of-mass anchoring with interaction between tip and one end of the dipole, and (c) center-of-mass anchoring with interaction between tip and both ends of the dipole. The light cyan arrows represent electrostatic forces due to the external field, while the darker red arrows are forces due to the interaction with the tip. The forces compete with one-another and must balance each other out to see the largest effects in the friction. Consequently, for different geometries the peak in the friction appears at different values of the external field.
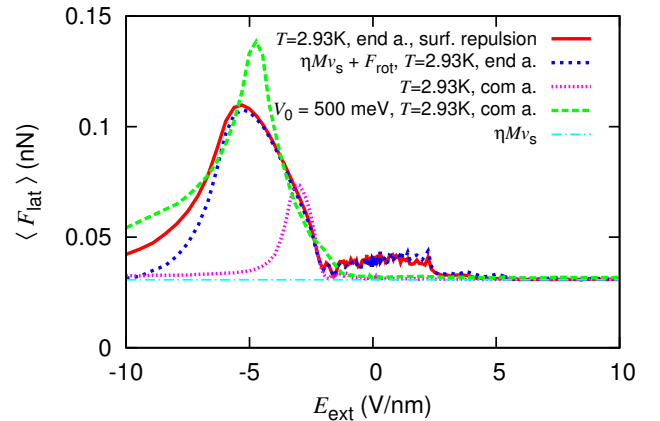
FIG. 7: Field-dependence of friction, comparison between center-of-mass and end anchoring for $V_0 = 250$ meV, and center-of-mass anchoring with $V_0 = 500$ meV. The peak in the friction for end anchoring with $V_0 = 250$ meV is close to the peak for center-of-mass anchoring with $V_0 = 500$ meV.

fectively partially cancelled out. This can be seen in the diagram in Fig. 6c. Consequently, the peak in the friction around the transition shifts towards weaker fields.

IV. FORCE CONSTANTS AND DISPERSION

We can gain further understanding of the geometric effects in the system and the differences between the two types of anchoring by considering the energy landscape in the absence of the tip as well as the resulting phonon dispersion. In this section we calculate the force constants for deviation from equilibrium for center-of-mass anchor-
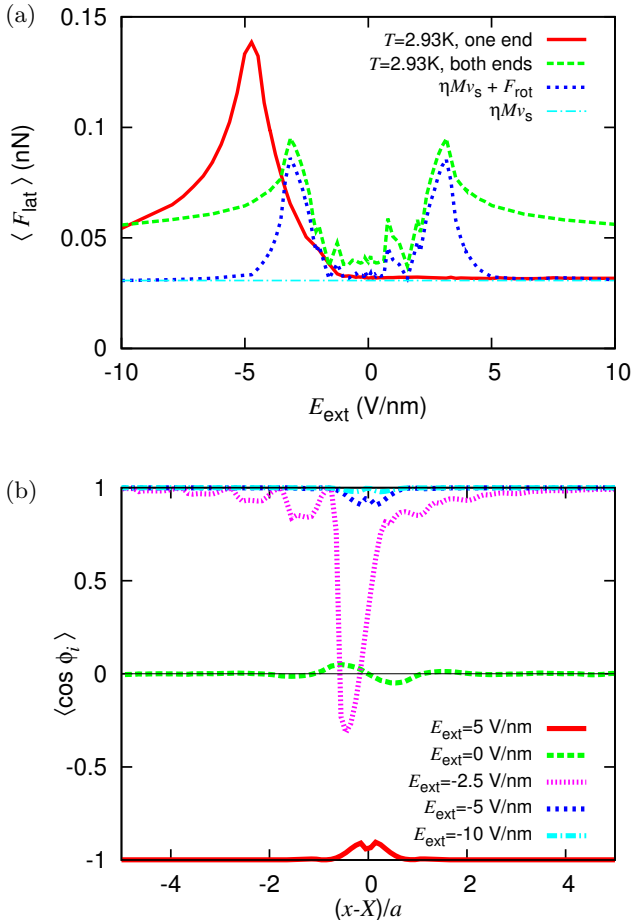
FIG. 8: Field-dependence of friction (a) and polarization as a function of the distance to the tip (b), for both ends of the dipole interacting with the tip.

ing and for end anchoring with negative fields, where the dipoles point out of the substrate and are not affected by the surface repulsion in the leading orders.

A. Force constants

First, we must linearise the system about its ground state. The force constants can be obtained by perturbing around the ground state and performing an expansion of the total energy of the dipoles without the tip, i.e. Eq. (5), and in the presence of the external field, i.e. with an extra term of $\sum_i dqE_{\text{ext}} \cos \phi_i$.

Let $V(\{\phi_i\})$ be the total potential energy of the system and let ϕ_i^0 denote the ground state. We may write

$$V(\{\phi_i\}) = V^{(0)} + \sum_i \tilde{V}^{(2)} \Delta\phi_i^2$$
$$+ \sum_{i,j \text{ nn}} V^{(2)} (\Delta\phi_i - \Delta\phi_j)^2 + \text{h. o.}, \quad (11)$$

where $\Delta\phi_i = \phi_i - \phi_i^0$. Here, $\tilde{V}^{(2)}$ and $V^{(2)}$ are the harmonic force constants for self-interaction and nearest-neighbour interaction respectively.

Under the assumption that in the ground state all dipoles point in the same direction $\phi_i^0 = \phi^0$, its total potential energy reduces to

$$V = Nq^2 \frac{1}{4\pi\epsilon_0\epsilon} \left[\frac{2}{a} - \frac{1}{\sqrt{(a + d\sin\phi^0)^2 + (d\cos\phi^0)^2}} \right.$$
$$\left. - \frac{1}{\sqrt{(a - d\sin\phi^0)^2 + (d\cos\phi^0)^2}} \right]$$
$$+ E_{\text{ext}} \sin\phi^0 . \quad (12)$$

Due to translation symmetry, this expression holds for both center-of-mass and end anchoring. The ground state is then found from the energy minimum, i.e. from $\partial V/\partial\phi^0 = 0$.

Taylor expansion then yields

$$\tilde{V}^{(2)} = \left[\frac{1}{2} dqE_{\text{ext}} \right.$$
$$\left. + \left(\frac{\partial^2}{\partial\phi_i^2} + \frac{\partial^2}{\partial\phi_i\partial\phi_j} \right) V_{\text{dipole}}(\phi_i, \phi_j) \right]\Bigg|_{\phi_i = \phi_j = \phi^0} , \quad (13)$$

$$V^{(2)} = -\frac{1}{2} \frac{\partial^2}{\partial\phi_i\partial\phi_j} V_{\text{dipole}}(\phi_i, \phi_j)\Bigg|_{\phi_i = \phi_j = \phi^0} . \quad (14)$$

As the equation for the ground state is transcendental, the force constants can only be obtained numerically. Results are plotted in Fig. 9 for both types of anchoring.

It can be seen from Fig. 9 that $V^{(2)}$ vanishes for some fields, indicating that, to leading order, there is no interaction between nearest neighbours. When this happens, energy cannot be redistributed through the chain so easily for dissipation. As a result, friction around these values of the field is reduced (see Fig. 4).

This point of vanishing friction is close to the peak in the friction in Fig. 4 for center-of-mass anchoring. Consequently, the peak is reduced on the right side, and fairly narrow (approximately 3 V/nm of full width at half hight after $\eta M v_s$ is subtracted). For end anchoring, the peak is further away from this point, in a regime where the nearest-neighbour coupling is nearly independent of the field (see Fig. 9). Consequently, the peak is broad (around 10 V/nm) and high. In the case of end anchoring with the weaker tip, when the peak is again around -5 V/nm, the effect is the same as for center-of-mass anchoring, the peak being narrow, with a width of approximately 4 V/nm, as can be seen in Fig. 7). We have investigated two more cases where the peak is even closer to the point of vanishing leading-order dipole-dipole interaction. These are a weak tip with center-of-mass anchored dipoles, and the normal tip interacting with both ends of the dipoles (Fig. 8). In these cases, the peak is even more narrow, 2 V/nm broad, and has even lower intensity.

There is also a range where $V^{(2)}$ is negative. As long as $\tilde{V}^{(2)} + 4V^{(2)} > 0$, nevertheless, the ground state with
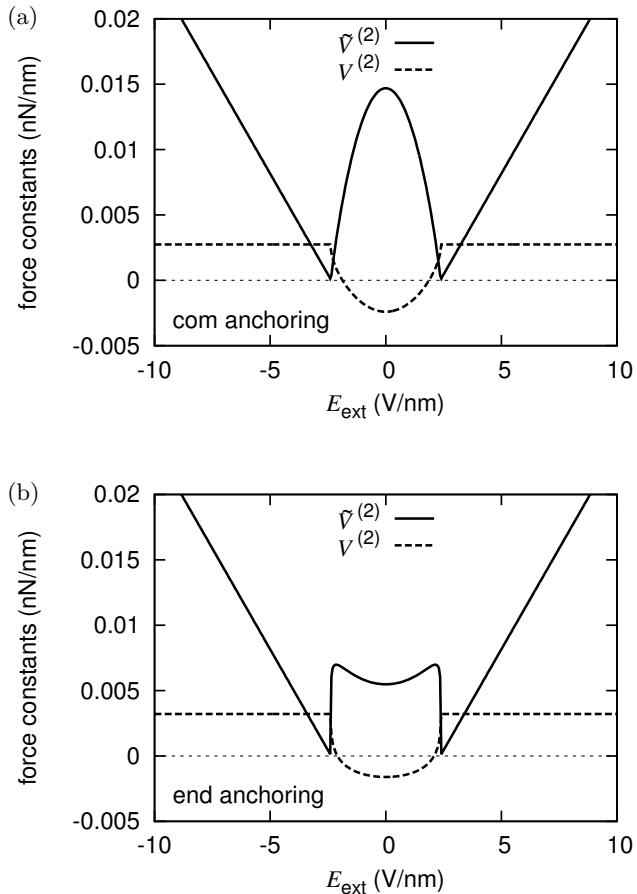
FIG. 9: Force constants for Eq. (11) for (a) center-of-mass and (b) end anchoring.

FIG. 10: Dispersion for (a) center-of-mass and (b) end anchoring, calculated using Eq. (16) and the force constants plotted in Fig. 9. There are several points where the dispersion becomes linear and low-frequency phonon modes become accessible.

all dipoles pointing in the same direction remains stable. If $\tilde{V}^{(2)} + 4V^{(2)} < 0$, however, this state is unstable. In this case the state $\Delta\phi_i = 0$ has higher energy than $\Delta\phi_{i+1} = -\Delta\phi_i \neq 0$, and there is a lower-energy ground state with dipoles pointing in two different alternating directions. Thus the assumption at the root of our calculation, that in the ground state all dipoles point in the same direction, is no longer valid. This does not happen for center-of-mass anchoring, but it happens for end anchoring at field strengths above -0.857 V/nm. The actual ground state consists of the dipoles pointing in two alternating, different, directions.

B. Phonon dispersion

Using the expansion of the force constants, we can linearise the equations of motion for the orientations of the dipoles, Eq. (3), around the ground state. Removing the terms for the tip and thermostat, we find

$$\ddot{\phi}_i = -\frac{2}{I}[\tilde{V}^{(2)}\Delta\phi_i - V^{(2)}(2\Delta\phi_i - \Delta\phi_{i+1} - \Delta\phi_{i-1})] . \tag{15}$$

This equation has periodic solutions of the form $\Delta\phi_i \propto \exp[2\pi i(kx_i + \omega(k)t)]$, which yield the phonon dispersion relation $\omega(k)$. We find

$$\omega(k) = \sqrt{[2\tilde{V}^{(2)} + 8V^{(2)}\sin(ka/2)^2]/I} . \tag{16}$$

This dispersion relation is plotted in Fig. 10 for the two different types of anchoring, and for different values of the external field.

For several values of the external field, the dispersion becomes (nearly) linear. This can be seen in Fig. 10. This means that the system has low-frequency phonon modes, which can absorb energy more easily, increasing dissipation.

One such point can be used to explain the peak in the friction around -1.7 V/nm seen in Fig. 4. From Eq. (16) and Fig. 9, we see that argument of the square root in Eq. (16) can become negative when $\tilde{V}^{(2)} + 4V^{(2)} < 0$. This happens only for end anchoring at field strengths above -0.857 V/nm, when also the state with all dipoles pointing in the same direction becomes unstable. At this

field strength, the dispersion is thus linear, as can be seen from the inverted linear dispersion shown in Fig. 10(b). The resulting low-frequency phonon modes lead to a strong, but narrow peak in the friction. This peak is shifted somewhat due to the surface repulsion and influence of the tip. Simulations without surface repulsion show the sharp peak around -0.9 V/nm.

There is another field strength that produces linear dispersion, namely -2.372 V/nm. This can be seen in Fig. 10 for both types of anchoring. This is due to the fact that $\tilde{V}^{(2)}$ vanishes very briefly. However, we did not observe a corresponding peak in the friction in our simulations. There is a sharp kink in $\tilde{V}^{(2)}$ precisely at the point where it vanishes, and its first derivative is very high. Furthermore, the point at which $V^{(2)}$ vanishes, reducing the friction, is very close by. As a result, the peak is likely to be extremely narrow.

V. CONCLUSIONS

We have used a simple model to investigated the effect of the molecule anchoring on the friction as a function of the applied potential near a reorientation transition. We consider adsorbed molecules which rotate around their center of mass as well as molecules which are anchored by one of their ends. We find that the peak in the friction is robust, but that it shifts relative to the transition and its width and height change. This shift can be explained

from the competition between two types of interactions: dipole-dipole interaction and dipole-tip interaction. We also consider the phonon dispersion in the dipole chain and use this to show how the width and height of the peak can be understood from features in the dipole-dipole interactions.

Our results show that the variation of friction with external electrical fields is strongly affected by the anchoring of adsorbed molecules. This provides insight into how the molecule anchoring can be used as for the creation of electrolyte-based lubricants with specific responses to external electric fields.

[1] Y. Y. Zhu, G. H. Kelsall, and H. A. Spikes, Tribology Transactions **37**, 811 (1994).
[2] Y. Meng, B. Hu, and Q. Chang, Wear **260**, 305 (2006).
[3] M. N. F. Ismail, T. J. Harvey, J. A. Wharton, R. J. K. Wood, and A. Humphreys, Wear **267**, 1978 (2009).
[4] A. Kailer, T. Amann, O. Krummhauer, M. Herrmann, and U. S. M. Schneider, Wear **271**, 1922 (2011).
[5] E. Weilandt, A. Menck, and O. Marti, Surf. Interface Anal. **23**, 428 (1995).
[6] M. Nielinger and H. Baltruschat, PCCP **9**, 3965 (2007).
[7] F. Hausen, M. Nielinger, S. Ernst, and H. Baltruschat, Electrochim. Acta **53**, 6058 (2008).
[8] A. Labuda, W. Paul, B. Pietrobon, R. B. Lennox, P. H. Grutter, and R. Bennewitz, Rev. Sci. Instrum. **81**, 083701 (2010).
[9] F. Hausen, N. N. Gosvami, and R. Bennewitz, Electrochim. Acta **56**, 10694 (2011).
[10] A. Labuda, F. Hausen, N. N. Gosvami, P. H. Grutter, R. B. Lennox, and R. Bennewitz, Langmuir **27**, 2561 (2011).
[11] F. Hausen, J. A. Zimmet, and R. Bennewitz, Surf. Sci. **607**, 20 (2013).
[12] R. Bennewitz, F. Hausen, and N. N. Gosvami, J. Mater. Res. **28**, 1279 (2013).
[13] M. Valtiner, K. Kristiansen, G. W. Greene, and J. N. Israelachvili, Adv. Mater. **23**, 2294 (2011).
[14] L. Stolberg, S. Morin, J. Lipkowski, and D. Irish, J. Electroanal. Chem. **307**, 241 (1991).
[15] W.-B. Cai, L.-J. Wan, H. Noda, Y. Hibino, K. Ataka, and M. Osawa, Langmuir **14**, 6992 (1998).
[16] S. Iqbal, S. Wezisla, N. Podgaynyy, and H. Baltruschat, Electrochimica Acta **186**, 427 (2015), ISSN 0013-4686, URL http://www.sciencedirect.com/science/article/pii/S0013468615305880.
[17] A. Vanossi, N. Manini, M. Urbakh, S. Zapperi, and E. Tosatti, Rev. Mod. Phys. **85**, 529 (2013).
[18] A. S. de Wijn, A. Fasolino, A. E. Filippov, and M. Urbakh, Phys. Rev. Lett. **112**, 055502 (2014).
[19] M. N. F. and R. J. Watts-Tobin, Electrochimica Acta **4**, 79 (1961).
[20] G. Nagy, K. Heinzinger, and E. Spohr, J. Chem. Soc., Faraday Discuss. **94**, 307 (1992).
[21] M. F. Toney, H. N. Howard, J. Richer, G. L. Borges, J. G. Gordon, O. R. Melroy, D. G. Wiesler, Y. D., and L. B. Sorensen, Nature pp. 444–446 (1994).
[22] K. Ataka, Y. T., and M. Osawa, J. Phys. Chem. **100**, 10664 (1996).
[23] W. Schmickler and E. Santos, *Interfacial Electrochemistry* (Springer, 2010).
[24] A. A. Kornyshev, in *The Chemical Physics of Solvation*, edited by R. R. Dogonadze, E. Kalman, A. A. Kornyshev, and J. Ulstrup (Amsterdam: Elsevier, 1986), pp. part C, 355–400.